

# Multiple structure of a laser-induced underwater shock wave

Yoshiyuki Tagawa,\* Shota Yamamoto, Keisuke Hayasaka, and Masaharu Kameda  
Department of Mechanical Systems Engineering, Tokyo University of Agriculture and Technology,  
Naka-cho 2-24-16, Koganei, Tokyo 184-8588, Japan  
(Dated: March 16, 2022)

The structure of a laser-induced underwater shock wave is examined. Plasma formation, shock-wave expansion, and temporal evolution of shock pressure are observed *simultaneously* using a combined measurement system that obtains high-resolution nanosecond-order image sequences. In contrast to a well-known spherical-shock model, these detailed measurements reveal a non-spherically-symmetric distribution of pressure peak for a wide range of experimental parameters. The structure is determined to be a collection of *multiple* spherical shocks originated from elongated plasmas.

*Introduction.*— Underwater shock waves induced by illumination with a nanosecond laser pulse are utilized in various applications including low-invasive medical treatments, such as laser lithotripsy [1–4] and needle-free injection devices [5–7]. Illumination with a laser pulse first triggers the emergence of plasma in water, which leads to rapid expansion of a bubble and emission of a shock wave [8, 9]. The structure of the shock wave has been commonly modeled as a *spherical shock*, which assumes a spherically-symmetric pressure distribution [10–13]. However, some researchers have pointed out that the spherical-shock model is not always applicable [14–16]. Sankin *et al.* [14] measured pressure peaks for a shock at various positions and determined that the peak pressure at a point in the direction perpendicular to the laser beam is more than twice as high as that in the direction of the laser. Noack and Vogel [15], Vogel *et al.* [16] reported that the shape of a shock wave is not always spherical due to conical plasma formation. Despite these considerations, a common model for the structure of laser-induced shock waves has not been developed.

In this Letter, we report on experimental observations of a laser-induced shock wave to clarify its structure. However, such an observation is challenging because each phenomenon involved in generating the shock occurs within a short time; the time scale for plasma growth is in the order of nanoseconds and the shock velocity in water is approximately 1500 m/s. To the best of the authors' knowledge, plasma growth, the expansion process of the shock, and temporal pressure evolution have been *simultaneously* measured for the first time, using a combined measurement system, in which ultra-high-speed recording systems and pressure sensors are installed.

*Experimental setup and method.*— Figure 1 shows the combined measurement system. An underwater shock wave is induced by a 532 nm, 6 ns laser pulse focused through an objective lens to a point inside a water-filled glass tank (100×100×450 mm). The input laser energy (2.6 mJ, 6.9 mJ, and 12.3 mJ) and the magnification of the objective lens (5×, 10×, and 20×) were varied.

The combined measurement system consists of two hydrophones (Muller Platte-Gauge, Muller Co.) and two ultra-high-speed cameras. One of the hydrophones is placed 5 mm away from the focal point of the laser in the direction of the laser beam ( $\theta = 0^\circ$  direction). The other hydrophone is at the same distance but in the direction perpendicular to the laser beam ( $\theta = 90^\circ$  direction). One of the cameras is an ultra-high-speed camera (Imacon 200, DRS Hadland Co.) with up to  $200 \times 10^6$  fps (5 ns time interval) and a  $1200 \times 980$  pixel array to record plasma formation. The other camera is another ultra-high-speed video camera (Kirana, Specialized Imaging Co.) with up to  $5 \times 10^6$  fps and a  $924 \times 768$  pixel array for imaging of shock-wave propagation. This camera is synchronized with a laser stroboscope that operates with a pulse width of 20 ns as a back illumination source (Cavilux Smart, Cavitar Co.), the repetition rate of which is also up to  $5 \times 10^6$  Hz. A digital delay generator (Model 575, BNC Co.) is used to trigger the laser, the hydrophones, the cameras, and the stroboscope. Each measurement was repeated more than three times under the same experimental conditions.

*Results and discussion.*— Figure 2 (in which  $t$  denotes the elapsed time from the start of illumination with the laser pulse) shows the measurement results obtained with the  $10 \times$  objective lens. Figure 2(i) shows a snapshot of the plasma luminescence in an elongated area, the major axis of which is in the direction of the laser beam. The image sequence of the plasma (see Supplementary Materials) suggests that all parts of the plasma emit strong light at the same time within  $\pm 5$  ns. A laser-induced bubble then emerges where the plasma was formed (Fig. 2(ii)) and its shape is also elongated in the direction of the laser beam. This bubble shape is similar to that reported by Vogel *et al.* [16]. At  $t = 0.4 \mu\text{s}$ , two overlapped spherical shocks are observed. In contrast, at  $t = 2.4 \mu\text{s}$ , the shock could be regarded as a single spherical shock (see Fig. 2(iii)). However, enlarged images for  $\theta = 0^\circ$  and  $\theta = 90^\circ$  (Fig. 2(iii)  $\theta = 0^\circ$  and  $\theta = 90^\circ$ ) display a clear difference. Two shock waves for  $\theta = 0^\circ$  (Fig. 2(iii)  $\theta = 0^\circ$ ), which is different from the single shock wave for  $\theta = 90^\circ$  (Fig. 2(iii)  $\theta = 90^\circ$ ). Figure 2(iv) shows the pressure evolution measured with the two hydrophones placed at different positions. There are two peaks for  $\theta = 0^\circ$ , while there is a single large peak for

\* tagawayo@cc.tuat.ac.jp

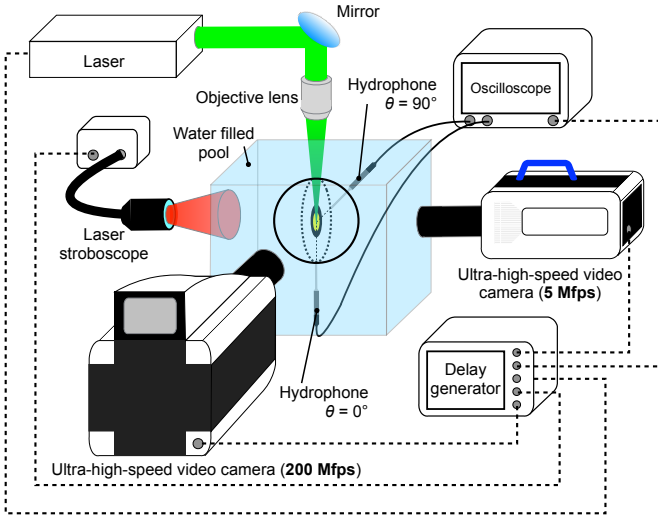


FIG. 1. Measurement system consisting of two ultra-high speed cameras and two pressure sensors. An ultra-high speed video camera records laser-induced shock waves and bubbles at up to  $5 \times 10^6$  fps with a synchronized laser stroboscope. Plasma luminescence is captured by another ultra-high speed video camera at up to  $200 \times 10^6$  fps. Temporal pressure evolution is measured by two hydrophones. One hydrophone is arranged in the direction of the laser beam ( $\theta = 0^\circ$ ) at a stand-off distance of ca. 5 mm from the laser focal point, while the other hydrophone is at right angles to the hydrophone ( $\theta = 90^\circ$ ) at the same stand-off distance.

$\theta = 90^\circ$ , which is approximately 1.3 times higher than that for  $\theta = 0^\circ$ . Note that this dependence of the peak pressure on the angle  $\theta$  is the same as that reported by Sankin *et al.* [14].

Figure 3 presents the measurement results for the  $5 \times$  objective lens. An elongated plasma is also observed in the direction of the laser beam, as shown in Fig. 3(i), which is similar to that observed with the  $10 \times$  objective lens (Fig. 2(i)). The luminescence area for the  $5 \times$  objective lens is much larger than that for the  $10 \times$  objective lens. Furthermore, for the  $5 \times$  objective lens, four plasma groups separated from each other are evident. At  $t=0.4 \mu\text{s}$  (Fig. 3(ii)) four spherical-shock waves are observed, the centers of which are in the areas where the plasma groups had emerged. At  $t=2.4 \mu\text{s}$  (Fig. 3(iii)), enlarged images of the shock show four shock waves for  $\theta = 0^\circ$  ((Fig. 3(iii)  $\theta = 0^\circ$ )) and a single shock wave for  $\theta = 90^\circ$  ((Fig. 3(iii)  $\theta = 90^\circ$ )). In Fig. 3(iv), the waveforms of the shock pressure are notably different between  $\theta = 0^\circ$  and  $\theta = 90^\circ$  observed with the  $5 \times$  objective lens. Four peaks are observed for  $\theta = 0^\circ$ , while a single large peak is observed for  $\theta = 90^\circ$ , which is approximately four times higher than that for the  $\theta = 0^\circ$  peaks. It is noted that the multiple generation of spherical-shock waves for the  $5 \times$  objective lens are much more pronounced than those for the  $10 \times$  objective lens.

Based on the aforementioned results, we here propose a model for the structure of the laser-induced shock wave:

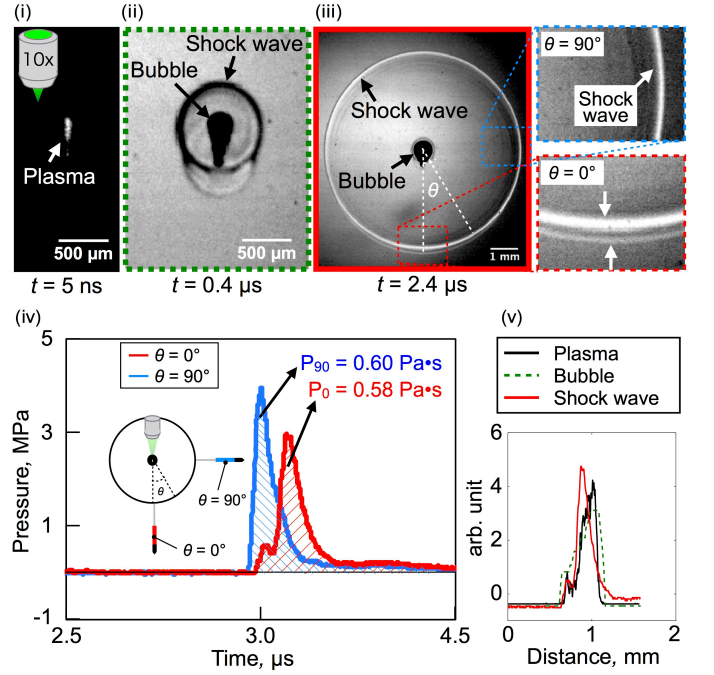


FIG. 2. Measurement results for a laser-induced underwater shock wave obtained with a  $10 \times$  objective lens. (i) Plasma luminescence at  $t = 5$  ns after the laser is fired. The image is captured by an ultra-high-speed video camera at 200 Mfps. (ii) Shock waves and bubbles at  $t = 0.4 \mu\text{s}$  imaged with an ultra-high speed video camera at 5 Mfps. (iii) Shock waves at  $t = 2.4 \mu\text{s}$  measured with an ultra-high-speed video camera at 5 Mfps. Enlarged images for the areas of  $\theta = 0^\circ$  and  $\theta = 90^\circ$  are also presented. (iv) Shock pressure measured by the two hydrophones arranged at  $\theta = 0^\circ$  (red line) and  $\theta = 90^\circ$  (blue line) with respect to the laser direction. Integrations for the pressure with respect to the elapsed time indicate pressure impulses. (v) Normalized waveforms for plasma luminescence, bubble width, and shock pressure as a function of distance.

The shock has a multiple structure that consists of multiple spherical shock waves as depicted schematically in Fig. 4. Each spherical shock wave originates from the corresponding plasma formation. For both the  $10 \times$  and  $5 \times$  objective lens, this model rationalizes the observations of several peaks for  $\theta = 0^\circ$  and the single large peak for  $\theta = 90^\circ$ .

To validate the multiple-structure model quantitatively, we compute the pressure impulse for  $\theta = 0^\circ$ ,  $P_0$ , and that for  $\theta = 90^\circ$ ,  $P_{90}$ . The definition of the pressure impulse is given as:

$$P = \int p dt, \quad (1)$$

where  $p$  is the shock pressure and  $t$  is the elapsed time. Given that the shock wave is in a linear system, we could apply the *superposition principle*: the net pressure that is produced by two or more shock waves reaching the same point is the sum of the pressure induced by the individual shock waves. Therefore,  $P_0$  would be in agreement

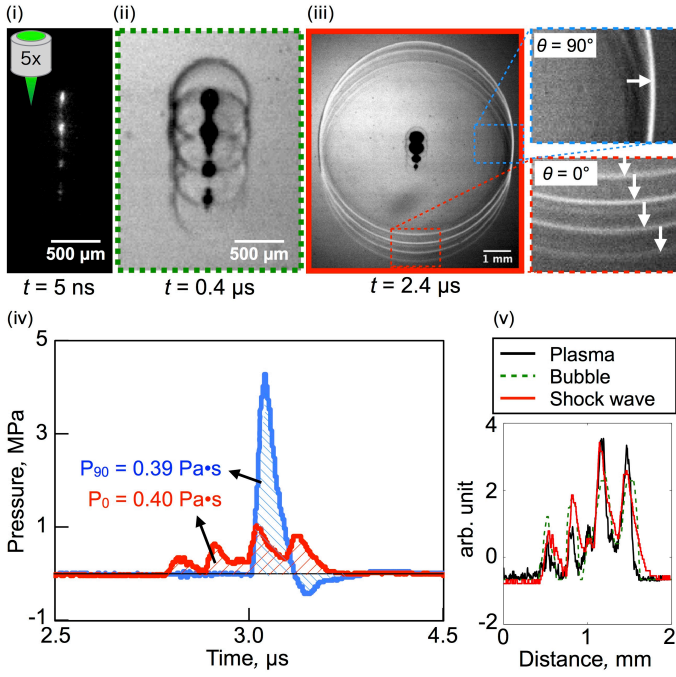


FIG. 3. Measurement results for a laser-induced underwater shock wave obtained with a  $5\times$  objective lens. Captions for (i)-(v) are the same as those in Fig. 2.

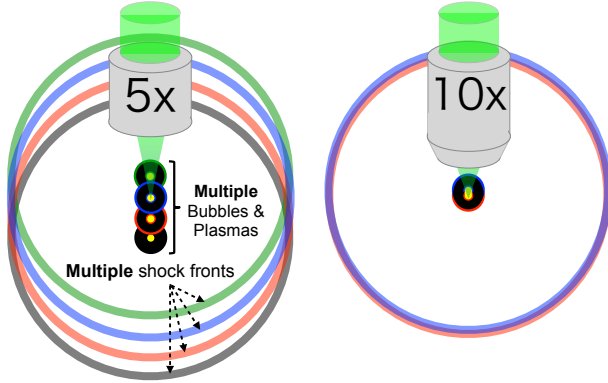


FIG. 4. Schematic of a multiple structure model for a laser-induced underwater shock wave. Multiple plasmas emit multiple bubbles and spherical shock waves. In a linear system, the shock pressure at a certain point is the sum of spherical shock pressures that reach the same point.

with  $P_{90}$  due to the superposition of multiple spherical shock waves. According to Fig. 2(iv) and Fig. 3(iv),  $P_0$  is in reasonable agreement with  $P_{90}$ . Furthermore,  $P_0$  and  $P_{90}$  were examined for all the other experimental conditions, i.e., different laser energy (2.6 and 12.3 mJ) and objective lens ( $20\times$ ) (data shown in Supplementary Materials). The  $P_0$  was in agreement with the corresponding  $P_{90}$  within the experimental uncertainty for a wide range of experimental parameters, even though the

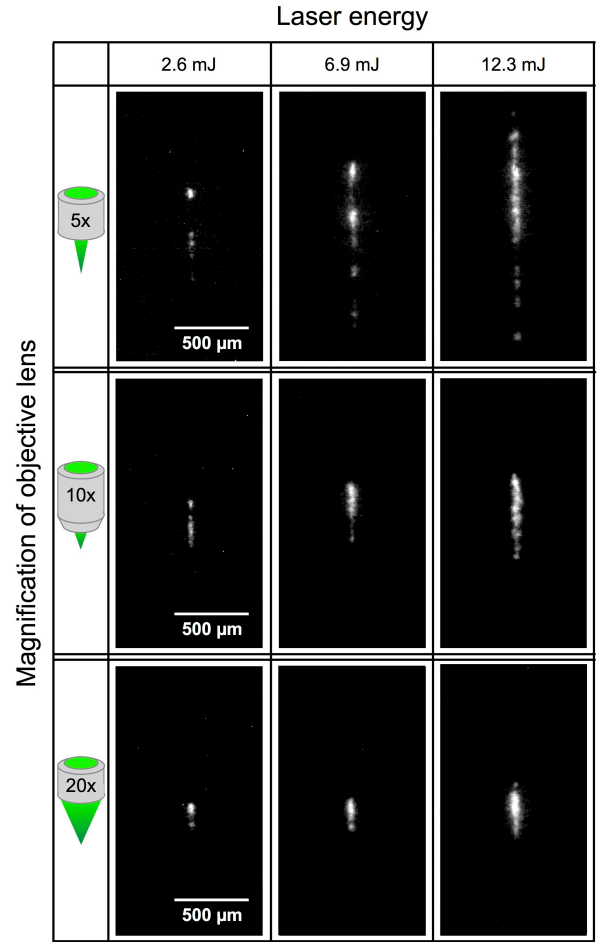


FIG. 5. Plasma formation under all experimental conditions (Magnification of objective lens:  $5\times$ ,  $10\times$ ,  $20\times$ . Laser energy: 2.6, 6.9, and 12.3 mJ). The plasma shape is the most elongated with an input energy of 12.3 mJ and the  $5\times$  objective lens, whereas it is rather spherical with an input energy of 2.6 mJ and the  $20\times$  objective lens.

pressure peaks for both  $\theta = 0^\circ$  and  $\theta = 90^\circ$  differ significantly. These agreements indicate the universality of the multiple structure model. It should be emphasized that, as observed with the  $10\times$  objective lens (Fig. 2), even if just a single plasma or a bubble is observed, the origin of the *elongated* plasma and bubble is expected to be multiple spots of plasma, which leads to the emergence of a multiple structure for the shock, which results in a notable angular variation of shock pressure.

Provided that all the spherical shock waves originate from simultaneous emergence of the plasmas, the waveform of the shock pressure would be strongly related to the plasma shape, as would that for the bubbles. For clear presentation, we focus on the results for  $\theta = 0^\circ$  and compare them as a function of the distance. For the plasma shape, we integrate the intensity of plasma luminescence in the lateral direction for the image obtained at  $t = 5$  ns. For the bubble shape, we measure

the bubble widths in the lateral direction for the image obtained at  $t = 0.4 \mu\text{s}$  as a function of distance. For the waveform of shock pressure, the elapsed time  $t$ , is translated into propagation distance by multiplying the time  $t$  by the shock velocity, 1483 m/s. For direct comparison, these three data are then normalized by their mean values and standard deviations. For the  $10\times$  objective lens, as shown in Fig. 2(v), the positions of peak pressure agree with those for the plasma shape and bubbles. The correlation coefficient between the shock pressure and bubble shape is 0.91, and that between the shock pressure and plasma shape is 0.87, which indicates a strong correlation between any two of the three quantities. For the  $5\times$  objective lens, there are also strong correlations; the correlation coefficients for pressure–bubble and for pressure–plasma are respectively 0.91 and 0.89. These agreements suggest a scenario where every spot of plasma generates a spherical shock wave and a bubble, the collection of which is what is observed in these experiments. Note that this scenario includes the well-known spherical-shock model. A phenomenon that is analogous to this may be the surface wave observed after one or several stones are thrown into a quiescent pond (the so-called Huygens–Fresnel principle).

Here, attention is given to plasma formation, which is the origin of the multiple shock structure. Figure 5 shows the plasma luminescence under all the experimental conditions. The shape of the plasma is dependent on both the magnification of the objective lens and the input laser energy. Plasma is generated where the energy density is locally enhanced [17]. As the input laser energy is increased, the region of plasma generation is enlarged more in the direction of the laser pulse beam, due to extension of the high energy density region. In the case of the  $5\times$  objective lens, the region of plasma generation is enlarged in the direction of the laser pulse beam, due to the small convergence angle (the maximum angle of the input laser beam to the optical axis). The regions of plasma generation with the  $10\times$  and  $20\times$  objective lens are smaller than that with the  $5\times$  objective lens because the convergence angles for the  $10\times$  and  $20\times$  objective lens are larger than that for the  $5\times$  objective lens.

The model for the multiple shock structure could possibly rationalize the results reported in previous research. For instance, Sankin *et al.* [14] reported that a laser-induced shock wave emitted from an elongated plasma

has an angular variation of pressure distribution. Although the shape of the shock wave appears to be spherical, the elongated plasma shape may cause a multiple-structure of the shock, as observed in the present experiments (see Fig. 2), which would lead to a non-spherically-symmetric pressure peak of the shock.

*Conclusion and Outlook.*— A measurement system consisting of a combination of ultra-high-speed cameras and pressure sensors was constructed to investigate the structure of a laser-induced shock wave. Shock pressure was measured with two hydrophones arranged at  $\theta = 0^\circ$  and  $\theta = 90^\circ$  with respect to the laser direction, and plasma formation and shock wave expansion were simultaneously observed using two ultra-high-speed video cameras. Based on these measurement results, we have proposed a multiple structure model for the laser-induced shock wave: The laser-induced shock wave is a collection of spherical shock waves emitted from the bright spots inside the area of plasma luminescence. The multiple structure is dependent on the plasma shape generated by illumination with the laser pulse.

As an outlook, by changing the plasma shape with control parameters (magnification of the objective lens or the input laser energy), the anisotropy of the shock pressure could be controlled, which might be applicable to a variety of advanced techniques. To achieve efficient low-invasive lithotripsy, for instance, kidney stones could be efficiently fractured using a high pressure peak of the shock for  $\theta = 90^\circ$ , while preventing damage of inward organs by maintaining a low peak pressure for the other  $\theta$ . It should be noted again that the multiple shock structure ensures the same pressure impulse in all directions. This feature may provide high degrees of freedom for the design of needle-free injection devices using high-speed microjets. Future numerical simulation based on the multiple-structure model is expected to provide additional support for this model. The limitation of the model is the assumption of a linear system. With very strong shock pressure ( $\gtrsim 100$  MPa [16]), the system becomes nonlinear, and the model is not applicable in its present form. Therefore, further studies are required to extend the current model for a nonlinear system.

*Acknowledgments.*— The authors thank Shu Takagi and Yoichiro Matsumoto for the use of the Imacon 200 ultra-high-speed camera. This work was supported by Kakenhi Grant-in-Aid (No. 26709007) from the Japan Society for the Promotion of Science (JSPS).

- 
- [1] H. A. Razvi, J. D. Denstedt, S. S. Chun, and J. L. Sales, *J. Urol.* **156**, 912 (1996).
  - [2] M. Sofer, J. Watterson, T. Wollin, L. Nott, H. Razvi, and J. Denstedt, *J. Urol.* **167**, 31 (2002).
  - [3] J. S. Lam, T. D. Greene, and M. Gupta, *J. Urol.* **167**, 1972 (2002).
  - [4] G. Sankin, W. Simmons, S. Zhu, and P. Zhong, *Phys. Rev. Lett.* **95**, 034501 (2005).
  - [5] V. Menezes, S. Kumar, and K. Takayama, *J. Appl. Phys.* **106**, 086102 (2009).
  - [6] Y. Tagawa, N. Oudalov, C. W. Visser, I. R. Peters, D. van der Meer, C. Sun, A. Prosperetti, and D. Lohse, *Phys. Rev. X* **2**, 031002 (2012).
  - [7] Y. Tagawa, N. Oudalov, A. El Ghalbzouri, C. Sun, and D. Lohse, *Lab Chip* **13**, 1357 (2013).
  - [8] J. Noack and A. Vogel, *IEEE Journal of Quantum Elec-*

- tronics **35** (1999).
- [9] W. Lauterborn, T. Kurz, C. Schenke, O. Lindau, and B. Wolfrum, IUTAM Symposium on Free Surface Flows, Fluid Mechanics and Its Applications **62**, 169 (2001).
- [10] C. J. Davie and R. G. Evans, Phys. Rev. Lett. **110**, 185002 (2013).
- [11] K. Ando, A.-Q. Liu, and C.-D. Ohl, Phys. Rev. Lett. **109**, 044501 (2012).
- [12] W. Lauterborn and A. Vogel, *Bubble Dynamics and Shock Waves* (Springer, 2013) pp. 67–103.
- [13] R. Petkovšek, J. Možina, and M. Griša, Opt. Express **13**, 4107 (2005).
- [14] G. N. Sankin, Y. Zhou, and P. Zhong, J. Acoust. Soc. Am. **123**, 4071 (2008).
- [15] J. Noack and A. Vogel, Appl. Opt. **37**, 4092 (1998).
- [16] A. Vogel, S. Busch, and U. Parlitz, J. Acoust. Soc. Am. **100**, 148 (1996).
- [17] A. Vogel, J. Noack, G. Hüttman, and G. Paltauf, Appl. Phys. B **81**, 1015 (2005).